IEEE Access
Multidisciplinary ⋮ Rapid Review ⋮ Open Access Journal

Received May 5, 2020, accepted May 25, 2020, date of publication June 1, 2020, date of current version June 19, 2020.

Digital Object Identifier 10.1109/ACCESS.2020.2998938

A Leakage-Based Directional Modulation Scheme for Frequency Diverse Array in Robot Swarm Networks

SHENG KE[1], (Graduate Student Member, IEEE), MINJUE HE[2], XIANGYUAN BU[1], (Member, IEEE), AND WENLONG CAI[3]

[1]School of Information and Electronics, Beijing Institute of Technology, Beijing 100081, China
[2]Science and Technology on Electronic Information Control Laboratory, Chengdu 610036, China
[3]National Key Laboratory of Science and Technology on Aerospace Intelligence Control, Beijing Aerospace Automatic Control Institute, Beijing 100854, China

Corresponding author: Minjue He (heminjue@139.com)

This work was supported by the National Natural Science Foundation of China under Contract U1836201 and Contract 6180011907.

ABSTRACT Robot swarms, which constitute typical multi-user systems, have played more and more important roles in many areas. In this paper, a directional modulation (DM) scheme for frequency diverse array (FDA) based on the leakage power minimization criterion is proposed, which can be used in a robot swarm system as well as other multi-user scenarios. Based on this scheme, location-dependent secure transmission can be obtained in the multi-user downlink channels under certain circumstances, where independent data streams can be sent to different legitimate users safely. Meanwhile, the difficulty for perfect eavesdropping is significantly increased compared with phased-array-based DM. We also use the block successive upper-bound minimization algorithm to optimize the frequency offsets of the array, and the algorithm can be effectively performed. This scheme utilizes the baseband model of the FDA, which is another contribution of this paper. It solves the problems brought by the time-varying nature of the FDA and reveals the distance-angle correlation of the FDA more fundamentally. Based on that, besides the proposed FDA-DM scheme, a novel multiple access technique, named as link division multiple access, is also preliminarily proposed. It allows the transmitter to distinguish multiple users in the same or proximal locations without the help of time division, frequency division, or code division. At last, numerical results are presented to verify the superiorities of LDMA and the proposed FDA-DM scheme.

INDEX TERMS Robot swarm, frequency diverse array, directional modulation, leakage, physical-layer security.

I. INTRODUCTION

With the development of robotics, the robot swarm, which consists of multiple collaborative robot members, has attracted wide attention in many different research areas [1]–[4]. Compared with an independent robot, robot swarms are robust to failure of individual members. Moreover, robots can replace humans to work in more dangerous places, collect and transmit data with higher efficiency, and complete more complex tasks [5], [6]. Because of these advantages, robot swarm has great potentials in the field of reconnaissance, exploration, emergency rescue, and military. Meanwhile, some substantial progress has been obtained in terms of hardware implementation, which promotes the development of robot swarms.

One key technology for robot swarms is *multi-user multiple-input-multiple-output* (MU-MIMO) downlink transmission. This is because, on the one hand, besides complying with local control laws, the robot members often need to receive control instructions or other information from the control center (or the leading robot) to work collaboratively. In this scenario, one transmitter needs to serve multiple receivers, transmitting different data streams to each of them. Utilizing the spatial redundancy provided by antenna arrays, the dominant transmitter can suppress co-channel interference in downlink transmission with the same frequency and at the same time slot, and without the need of orthogonal user codes. That is why robot swarms constitute typical MU-MIMO systems. On the other hand, due to the

The associate editor coordinating the review of this manuscript and approving it for publication was Jiankang Zhang.

particularity and sensitivity of many applications, robot swarms often require secure wireless communication. The spatial freedom provided by MIMO can further expand the quality difference between legitimate channels and eavesdropping channels, thus provide better security performance. This technology is also known as *physical-layer security* (PLS).

In the past several years, PLS combined with *frequency diversity array* (FDA) has become one of the hottest issues in the field of secure communications. This is because the beam pattern of FDA is not only angle-dependent but also range-dependent by controlling the carrier frequencies at different antennas, which overcomes the limitation of the traditional arrays (such as *phased array* (PA), polarization-sensitive array, etc.) that only angle-dependent security can be provided. Based on this characteristic, recent theoretical researches naturally combined FDA with *directional modulation* (DM) [7], [8], the purpose of which is to realize point-to-point keyless secure transmission. Unfortunately, the range-dimension security provided by FDA is over-estimated since electromagnetic waves always propagate in a straight line, as well as the 'secure area'. This limitation was preliminarily revealed in [9], where the FDA's steering vector in Eq.(3) was essentially not related to range anymore. In a very recent study [10], the researchers elaborated on the security defects of FDA-DM in the range dimension systematically. The reason why the previous researches are wrong or only valid for a specific moment is that researchers have ignored the time-varying nature of the FDA's beam pattern. Recently, many pieces of research claimed that FDAs with time-modulated frequency offsets could generate time-invariant beam pattern [11]. However, time-variant frequency offsets make the implementations of the FDA more complex. Meanwhile, [12] pointed out if the beam pattern of FDA was time-invariant, it was no more range-dependent either. In short, due to the confusing time-varying nature of the existing model, there are many problems in the field of FDA-based secure communications.

To solve the mentioned problems, the conclusion is proposed for the first time in this paper that the FDA's baseband model should be used in communication systems. This will have a profound impact on future researches based on FDA. Perhaps affected by the early FDA-based radar system, the previous researches widely used the *radio frequency* (RF) model, which was not suitable in the communication systems. This is because the useful information is distributed in each sub-band. In order to extract useful signals and eliminate the impact of multi-carrier, the multi-band signals should be down-converted to baseband separately before further processing. The baseband model of the FDA is also angle-range-dependent, while simultaneously dependent on the clock difference between the transmitter and the receiver. Besides, the baseband model eliminates the time-varying nature of the FDA's RF model, which implies that neither the time-modulated weights nor frequencies are necessary for FDA-based beamforming or DM. Compared with the relevant researches based on the RF model [9], [13], [14], our proposed model greatly enhances the practicality of the FDA in communication systems.

Based on the baseband model, FDA-DM still has many advantages. The first is that the difficulty of being eavesdropped on useful information along the desired direction has increased significantly compared with PA-based DM. In addition, because the energy of the FDA's transmission signal is dispersed in multiple sub-bands, the transmission signal of an FDA has a lower power spectral density than that of a PA when the transmission power is the same. This characteristic is similar to spectrum spread [15], and can hide the transmitted signal under the environment noise, thus can realize low detection probability communication. Moreover, although FDA cannot provide absolute security in the distance dimension, the provided ''location-dependent'' differentiation can be utilized by the cooperative legitimate receivers. Especially when there are multiple legitimate users in the same direction, these users will suffer from severe multiple access interference when a traditional array is used, while FDA can suppress most of these interferences, thereby significantly increasing the capacity of the multi-user communication system.

Against the background, this paper introduces FDA-DM to downlink multi-user MIMO channels for the first time, which is very suitable for robot swarms to improve the efficiency of downlink communication. The main contributions of our research are summarized as follow:

- We established the baseband model of the FDA, which is time-invariant and depends both on the receiver's position and clock difference. Compared with the traditional time-varying RF model, the baseband model reveals the distance-angle correlation of the FDA more fundamentally and provides a new direction for future FDA-based researches.
- A novel multiple access scheme, named as *Link Division Multiple Access* (LDMA), is preliminarily proposed based on the FDA's baseband model. It allows multi-user access at the same time, with the same frequencies and without the use of orthogonal user codes, even when several users are in the same position or very close to each other.
- A multi-user downlink communication scheme based on FDA-DM is proposed, and the carrier frequencies of the FDA are optimized based on the criterion of leakage power minimization. In this scheme, the frequency offsets and the beamforming coefficients are time-invariant. Compared with PA and FDA with fixed frequencies, the proposed scheme achieves the highest sum secrecy rate. Meanwhile, it outperforms other beamforming technologies when there are unknown eavesdroppers.

The rest of this paper is organized as follows: in Section II, the baseband model of the FDA is established. Based on this model, the concept and a simple example of LDMA

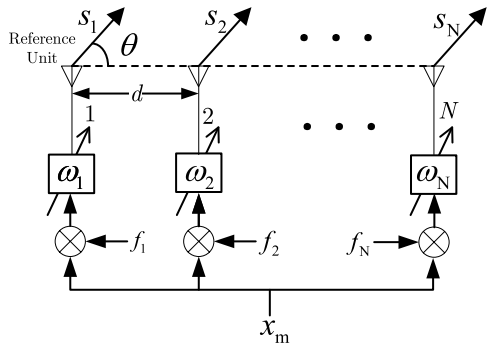

FIGURE 1. The model of an *N*-element uniform linear FDA.

are presented in Section III. In Section IV, the FDA-DM technique in the multi-user downlink network is proposed first. Then the optimization problem with respect to (w.r.t.) the FDA's frequency offsets is established, and an optimal solution is also provided. Besides, the sum secrecy rate of our proposed scheme is analyzed. Numerical simulation results and corresponding discussions are presented in Section V. Finally, we conclude our research in Section VI.

Notations: Throughout this paper, normal letters represent scalar variables, boldface lowercase letters represent vectors, and boldface capital letters represent matrices. $\mathbb{R}^{N\times M}$ and $\mathbb{C}^{N\times M}$ represent the real and complex domains of dimension $N \times M$, respectively. $(\cdot)^*$, $(\cdot)^T$ and $(\cdot)^\dagger$ denote conjugate operator, transpose operator and conjugate transpose operator, respectively. span$\{\boldsymbol{a}_1, \cdots, \boldsymbol{a}_N\}$ is the subspace spanned by $\boldsymbol{a}_1, \cdots, \boldsymbol{a}_N$. $\mathbf{0}_N$ is an N-dimensional zero vector. $\boldsymbol{I}_N$ is an N-dimensional identity matrix. $\lfloor a \rfloor$(or $\lceil a \rceil$) represents the smallest (or the largest) integer which is greater (or smaller) than a. $\{x\}_a^b$ represents the projection of x on the interval $[a, b]$. $a(t) * b(t)$ represents the convolution of $a(t)$ and $b(t)$. $|a|$ is the modulus of a and $\|\boldsymbol{a}\|$ is the Euclidean norm of the vector $\boldsymbol{a}$. sgn$\{x\}$ returns the sign of x. $\mathbb{E}\{\cdot\}$ represents taking expectation of random variables. $f'(x)$ and $f''(x)$ represent the first and the second derivative of $f(x)$, respectively.

II. THE BASEBAND MODEL OF FDA

Our discussion mainly focus on an N-element uniform linear FDA with equal spacing d, as illustrated in Fig.1. The similar discussions can readily be extended to arbitrary array structures. Unlike a PA that uses only a single carrier, FDA superimposes a small *frequency offset* (FO) on the basic carrier frequency for each element, i.e., $f_l = f_c + \Delta f_l$, where f_c is the basic carrier frequency and much higher than Δf_l. Denote $\boldsymbol{f} = [f_1, f_2, \cdots, f_l]^T$. To avoid multiple mainlobes, the spacing d should be no greater than $\lambda_{\min}/2$, where $\lambda_{\min}$ represents the wavelength corresponding to the highest frequency. Without loss of generality, the array antennas are assumed to be isotropic omnidirectional, and the first of them is set as the reference element. Denoting the beamforming coefficients as $\boldsymbol{\omega} = [\omega_1, \ldots, \omega_N]^T \in \mathbb{C}^{N\times 1}$, the transmitted signal of the FDA's lth element at the time interval t is

$$s_l(t) = x_m \omega_l e^{\mathrm{j}2\pi f_l t}, \quad l = 1, \ldots, N. \tag{1}$$

where x_m is the mth symbol carrying confidential information, satisfying $\mathbb{E}\{|x_m|\}^2 = 1$. When the far-field condition can be satisfied, with the line-of-sight and flat fading assumption, the received signal of a single receiving antenna at (R, θ) at time t can be expressed as

$$\begin{aligned} r(R,\theta,t) &\approx h(R)\sum_{l=1}^{N} s_l\left(t - \frac{R-(l-1)d\cos\theta}{c}\right) + \hat{n}(t) \\ &\approx h(R) x_{\lfloor m - \frac{R}{cT_s}\rfloor} e^{\mathrm{j}2\pi f_c\left(t-\frac{R}{c}\right)} \tilde{\boldsymbol{a}}^\dagger(R,\theta,t)\boldsymbol{\omega} + \hat{n}(t) \end{aligned} \tag{2}$$

where $h(R)$ is the channel coefficient, $c \approx 3 \times 10^8$m/s is the propagation speed of light, T_s is the symbol period, $\hat{n}(t) \sim \mathcal{CN}(0, \hat{\sigma}_n^2)$ is the additive white Guassian noise, and

$$\tilde{\boldsymbol{a}}(R,\theta,t) = \begin{bmatrix} e^{-\mathrm{j}2\pi\left(f_c\frac{0\cdot d\cdot\cos\theta}{c} + \Delta f_1\left(t-\frac{R}{c}\right)\right)} \\ e^{-\mathrm{j}2\pi\left(f_c\frac{1\cdot d\cdot\cos\theta}{c} + \Delta f_2\left(t-\frac{R}{c}\right)\right)} \\ \vdots \\ e^{-\mathrm{j}2\pi\left(f_c\frac{(N-1)\cdot d\cdot\cos\theta}{c} + \Delta f_N\left(t-\frac{R}{c}\right)\right)} \end{bmatrix} \tag{3}$$

is the steering vector of FDA, where the items $\Delta f_l(ld\cos\theta)/c$ are omitted due to the fact that $\Delta f_l \ll f_c$. Therefore, the array factor of FDA is defined as [16]

$$\mathrm{AF}(R,\theta,t) = \tilde{\boldsymbol{a}}^\dagger(R,\theta,t)\boldsymbol{\omega} \tag{4}$$

which is both angle and range dependent, while simultaneous varies with time. In this research, we focus on that all the receivers are equipped with a single antenna.

The RF model of the FDA in Eq.(3) is widely used in the communication systems. However, there are two problems in some studies: one is that the time-varying nature of the FDA has been ignored [7], [8], [17], so that the corresponding conclusions are only valid for a specific time interval, e.g., $t = 0$. The other is that time-modulated frequency or beamforming weights have to be used to obtain time-invariant performance [9], [13], [14], [18]. This makes the systems far more complicated and makes the analysis very error-prone. For example, in Eq.(8) of [13], the received signal should be $\boldsymbol{h}_L(\boldsymbol{f}, t)^H \boldsymbol{s}(t - \frac{r_L}{c})$, not as in the original text.

The reason why the previous studies used FDA's RF model extensively may be due to FDA's earlier applications in radar systems [19], where designing the beampattern is much more important than recovering the carried information. Whereas, it is not appropriate to directly analyze the FDA's RF model in the communication system. Similarly, the FDA-based beamforming technique should not be applied to communication systems directly. This is because even for the systems using a single tone, the corresponding receivers cannot extract symbols from the RF signals directly, but have to down-convert the signal to baseband before processing, not to mention those systems using multiple sub-bands. Most FDA-related research for communications ignored this point. On the other hand, Eq.(2) describes the received signal at time t, while the transmitted signal at time t should be received by the receiver

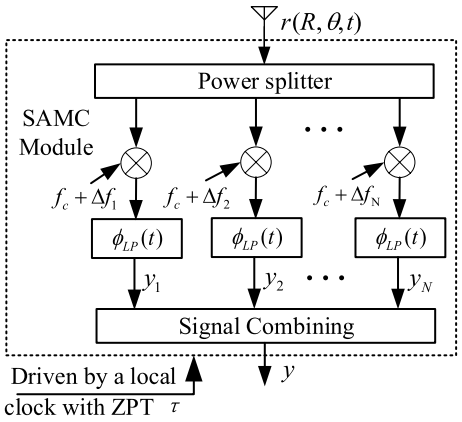

FIGURE 2. A single-antenna-multiple-channel receiver.

at time $t + \frac{R}{c}$. It is easy to verify that $r(R, \theta, t + \frac{R}{c})$ is not more related to R, which reveals that the RF model cannot explain well whether FDA still can provide range-dependent discrepancy in the communication systems.

To solve these problems, this paper will establish the baseband model of the FDA for the first time. To this end, we use the *single-antenna-multiple-channel* (SAMC) structure to process the received signal, which is illustrated in Fig.2. To facilitate the subsequent descriptions, we define *zero-phase-time* (ZPT) as the moment when the phases of all the subcarriers are 0. Without loss of generality, the ZPT of the transmitter is always set as 0, as given in Eq.(1), and the ZPT of the receiver is assumed to be τ. Then, by letting $m_R = \left\lfloor m - \frac{R}{cT_s} \right\rfloor$, the output of the SAMC module is

$$\begin{aligned} y(t) &= \sum_{l=1}^{N} \left[r(R, \theta, t) e^{-\mathrm{j}2\pi f_l (t-\tau)} \right] * \phi_{\mathrm{LP}}(t) \\ &= h(R) \sum_{l=1}^{N} \omega_l e^{\mathrm{j}2\pi \left(f_c \frac{(l-1) d \cos\theta}{c} - \Delta f_l \frac{R}{c} + f_l \tau \right)} + n(t) \\ &= h(R) x_{m_R} e^{\mathrm{j}2\pi f_c \tau} \boldsymbol{a}^{\dagger}(R, \theta, \tau) \boldsymbol{\omega} + n(t) \end{aligned} \tag{5}$$

where $\phi_{\mathrm{LP}}(t)$ is the unit impulse response of an ideal low-pass filter.

In Eq.(5), x_{m_R} and $n(t)$ must be time-varying, and $\boldsymbol{\omega}$ may be time-varying according to actual demands. $n(t) \sim \mathcal{CN}(0, \sigma_n^2)$ is the baseband noise, where σ_n can be explicitly calculated from $\hat{\sigma}_n$. $e^{\mathrm{j}2\pi f_c \tau}$ affects all sub-bands, so it eventually causes rotation of the constellation rather than distortion, which can be easily eliminated without affecting the communication process. Moreover, $\boldsymbol{a}(R, \theta, \tau)$, which is defined as

$$\boldsymbol{a}(R, \theta, \tau) = \begin{bmatrix} e^{-\mathrm{j}2\pi \left(f_c \frac{0 \cdot d \cdot \cos\theta}{c} + \Delta f_1 \left(\tau - \frac{R}{c} \right) \right)} \\ e^{-\mathrm{j}2\pi \left(f_c \frac{1 \cdot d \cdot \cos\theta}{c} + \Delta f_2 \left(\tau - \frac{R}{c} \right) \right)} \\ \vdots \\ e^{-\mathrm{j}2\pi \left(f_c \frac{(N-1) \cdot d \cdot \cos\theta}{c} + \Delta f_N \left(\tau - \frac{R}{c} \right) \right)} \end{bmatrix} \tag{6}$$

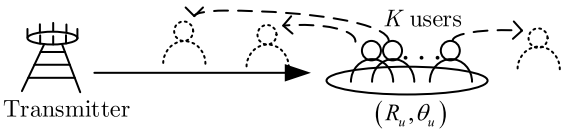

FIGURE 3. The system model of LDMA.

is the baseband model of the FDA. The baseband model of the FDA is still range and angle dependent, and it also depends on the clock difference between the sender and receiver. The model is no longer time-varying, while on the other hand, the distance and clock difference are coupled together in Eq.(6), i.e., $\boldsymbol{a}(R, \theta, \tau) = \boldsymbol{a}(0, \theta, \tau - \frac{R}{c})$. Therefore, this model does not violate the physical law of electromagnetic wave propagation. From another aspect, the reason why Eq.(6) is still related to R is that the receiver is not **ideally synchronized**. If the receiver is ideally synchronized, its ZPT should be $\frac{R}{c}$. In this case, the baseband signal no longer depends on R, only related to θ. This reveals that ideal synchronization underutilizes the spatial/time discrimination provided by the FDA. Aware of that, FDA can clearly provide more opportunities than traditional arrays in communication systems.

Admittedly, it is not the first time for SAMC receivers to be used in the FDA-based communication systems. The SAMC receiver was also used in [20], [21] to eliminate the time-varying nature of the FDA. However, the researchers did not realize that the **fully synchronized** assumption was used in these works, i.e., the ZPT of the receiver was also 0. Besides, we have to point out that the moments of the two down-conversions in Eq.(4) and (6) of [20], as well as in Eq.(3) and (6) of [21], were inconsistent. To the best of the authors' knowledge, our work reveals the relationship between the FDA's baseband model and the clock difference between the transmitter and the receiver for the first time, which may greatly promote the development of the FDA.

III. AN APPLICATION OF FDA: LINK DIVISION MULTIPLE ACCESS

Based on the baseband model, we will briefly introduce an application of the FDA. According to Eq.(5), FDA establishes a **virtual link** between the baseband signals of the transmitter and the receiver, which depends on not only the location, but also the ZPT of the receiver. It is quite conceivable that by adjusting the ZPTs of different users, the FDA can even distinguish between multiple users located at the same or proximal positions. This is the motivation of *link division multiple access* (LDMA), which allows multiple users to achieve code-free co-frequency communications during the same time interval. It has many similarities with *space division multiple access* (SDMA) and is also compatible with other *multiple access* (MA) technologies. However, the difference between LDMA and SDMA is that LDMA can distinguish multiple users in the same location.

We use a simple example to illustrate the principle of FDA-LDMA: consider the situation where K users are in the same location (R_u, θ_u), as shown in Fig.3. SDMA cannot

distinguish these users directly, and can only achieve multiple access through time division, frequency division, or code division. However, when the ZPTs of these users are different, FDA-LDMA can distinguish them without relying on other MA technologies. To be more specific, denote the ZPT of the kth user is τ_k. Since cooperative communication is considered, we assume that different users have different ZPTs, and the transmitter perfectly knows the *channel state information* (CSI) of all the users. The CSI of the receivers can be obtained through various channel estimation methods, e.g., [22], [23]. Denote the data stream and the weighting vector for the kth user as $x_{k,m}$ and $\boldsymbol{\omega}_k$ respectively, where $\mathbb{E}\{|x_{k,m}|^2\} = 1$. According to Eq.(5), the received baseband signal of the kth user is

$$y_k(t) = \underbrace{h(R_u)\, e^{\mathrm{j}2\pi f_c \tau_k} \boldsymbol{a}^{\dagger}(R_u, \theta_u, \tau_k)\, \boldsymbol{\omega}_k x_{k,m_{R_u}}}_{\text{desired signal}} + \underbrace{h(R_u) \sum_{\substack{n=1 \\ n\neq k}}^{K} e^{\mathrm{j}2\pi f_c \tau_k} \boldsymbol{a}^{\dagger}(R_u, \theta_u, \tau_k)\, \boldsymbol{\omega}_n x_{n,m_{R_u}} + n_k(t)}_{\text{Multiple Access Interference(MAI)}} \tag{7}$$

For the convenience of the subsequent derivations, *maximal ratio transmission* (MRT) weightings are assumed to be used by the transmitter, i.e., $\boldsymbol{\omega}_k = \sqrt{\frac{P_k}{N}}\boldsymbol{a}(R_u, \theta_u, \tau_k)$. Therefore, the system capacity of FDA-LDMA is given as [24]

$$C_{\mathrm{LDMA}} = \sum_{k=1}^{K} \log_2(1 + \gamma_k) \tag{8}$$

where γ_k is the *signal-to-interference-noise-ratio* (SINR) of the kth user, which can be expressed as

$$\gamma_k = \frac{NP_k\, |h(R_u)|^2}{|h(R_u)|^2 \sum\limits_{\substack{n=1 \\ n\neq k}}^{K} P_n \left|\boldsymbol{a}^{\dagger}(R_u, \theta_u, \tau_k)\, \boldsymbol{a}(R_u, \theta_u, \tau_n)\right|^2 + N\sigma_n^2} \tag{9}$$

On the other hand, as to SDMA which only depends on the locations of the users, it is easy to prove that the SINR of the kth user is

$$\tilde{\gamma}_k = \frac{P_k\, |h(R_u)|^2}{|h(R_u)|^2 \sum\limits_{\substack{n=1 \\ n\neq k}}^{K} P_n + \sigma_n^2} \tag{10}$$

According to the Cauchy-Schwartz inequality, it is obviously that $\tilde{\gamma}_k \leq \gamma_k$, which means SDMA suffers from more severe MAI. The relationship between the number of users K and the system capacities of SDMA and LDMA technologies is given in Fig.4, where $N = 4$, $f = 10\mathrm{GHz}+[0, 0.5, 0.8, 1.0]^T\mathrm{MHz}$, $R_u = 10\mathrm{km}$, $\theta_u = 90°$, $\tau_k = (k-1)\mathrm{us}$, $P_k = 1\mathrm{W}$ and $\sigma_n^2 = -30\mathrm{dBm}$. $h(R)$ is determined by the freespace path loss formula of radio wave propagation, which will be given in Eq.(36). Unsurprisingly,

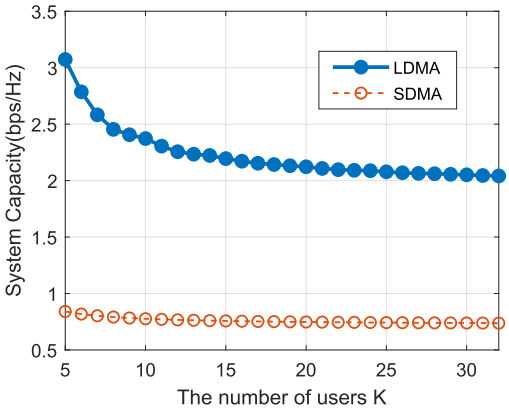

FIGURE 4. The system capacity comparison between LDMA and SDMA, where $N = 4$.

LDMA always achieved much higher system capacities than SDMA.

The advantage of FDA-LDMA has a physical explanation: as the range R and the clock difference τ are coupled together in the FDA's baseband model, changing the ZPTs of the users is equivalent to changing the locations, as illustrated in Fig.3, while the fading coefficient $h(R)$ keeps unchanged. Therefore, the transmitter can distinguish these users better thus the MAIs are suppressed. It is worth noting that although in this paper LDMA is realized based on FDA, LDMA may have more methods to be implemented, such as via multi-frequency arrays, etc. Moreover, better performance can certainly be achieved by diligently designing the weightings and the ZPTs of LDMA. In summary, LDMA still needs more further researches, which is beyond the scope of this thesis, so we only give a brief introduction and simply show the potential of LDMA in this section.

IV. FDA-BASED DM IN MULTI-USER DOWNLINK CHANNELS

A. LEAKAGE-BASED OPTIMIZATION FOR FDA-DM

In this section, we turn back to the theme of FDA-DM-based secure transmission technology in the multi-user system. Consider a downlink multi-user environment with a control center or a leading robot communicating with K followers, as well as E eavesdroppers. The transmitting array is of N elements, where N is required to be larger than K. All the receivers are equipped with a single antenna. A block diagram of the system is given in Fig.5. The transmitter sends independent data stream to each user, where $x_{k,m}$ is the mth symbol sent to the kth user. This is the difference between this paper and [14], where a broadcasting system was considered. Without loss of any generality, we assume that different legitimate users located at different places, denoted as $(R_{u,k}, \theta_{u,k})$, while all of them are fully synchronized with the transmitter. The fully-synchronized clocks between the transmitter and the users can be obtained through training or from a satellite navigation system like GPS [25]. On the other hand, the location of the kth eavesdropper is $(R_{e,k}, \theta_{e,k})$, and its ZPT is τ_k. We assume that the CSI of all the users is

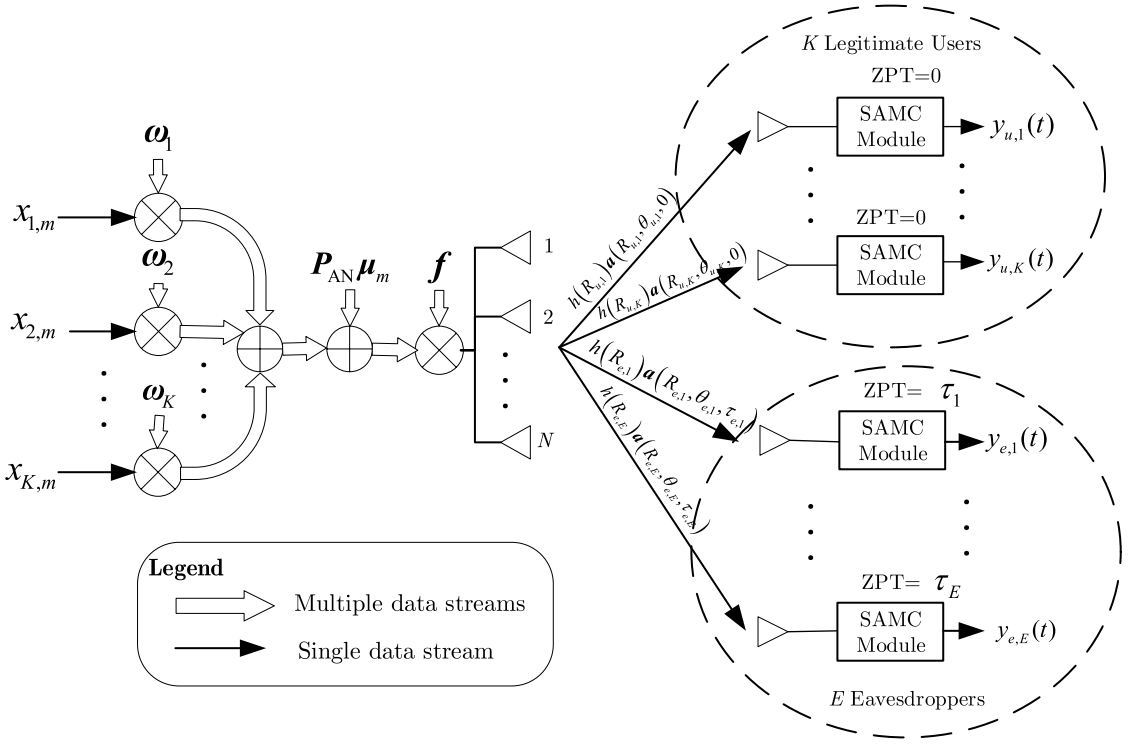

FIGURE 5. Block diagram of MU-MIMO wireless communication system based on FDA.

perfectly known by the transmitter. Moreover, with the help of DM that it can work without the prior knowledge of the eavesdroppers [26], we assume that only E_n eavesdroppers' CSI is known, where $0 \leq E_n \leq E$. According to the principle of the vector approach [26], the transmitted FDA-DM baseband signal vector at time t can be designed as

$$\boldsymbol{s}(t) = \sum_{k=1}^{K} \alpha_k \sqrt{P_s} \boldsymbol{\omega}_k x_{k,m} + \alpha_{\mathrm{AN}} \sqrt{P_s} \boldsymbol{P}_{\mathrm{AN}} \boldsymbol{\mu}_m \tag{11}$$

where P_s is the total transmit power, α_k and α_{AN} are real power allocating coefficients satisfying $\sum_{k=1}^{K} \alpha_k^2 + \alpha_{\mathrm{AN}}^2 = 1$. $\boldsymbol{\omega}_k$ is the beamforming coefficients corresponding to the kth data stream, which satisfies $\|\boldsymbol{\omega}_k\| = 1$. $\boldsymbol{P}_{\mathrm{AN}}\boldsymbol{\mu}_m$ constitutes the *artificial noise* (AN) excitation vectors, where $\boldsymbol{P}_{\mathrm{AN}} \in \mathbb{C}^{N\times(N-K)}$ is the unit orthogonal basis of the null space of span $\left\{\boldsymbol{a}\left(R_{u,1},\theta_{u,1},0\right),\cdots,\boldsymbol{a}\left(R_{u,K},\theta_{u,K},0\right)\right\}$. $\boldsymbol{\mu}_m \sim \mathcal{CN}\left(\boldsymbol{0}_{N-K}, \frac{1}{\sqrt{N}}\boldsymbol{I}_{N-K}\right)$ consists of $N-K$ independent and identically distributed Gaussian random variables, and is updated at the symbol rate. Because the baseband model of FDA is time-invariant, we abbreviate $\boldsymbol{a}\left(R_{u,k},\theta_{u,k},0\right)$ as $\boldsymbol{a}_{u,k}$, and $\boldsymbol{a}\left(R_{e,k},\theta_{e,k},\tau_k\right)$ as $\boldsymbol{a}_{e,k}$. We also drop the time notation t, as well as the symbol index subscript m and m_R for notation simplicity. Therefore, the baseband received signal of User k can be expressed as

$$y_{u,k} = \alpha_k \sqrt{P_s} h_{u,k} \boldsymbol{a}_{u,k}^{\dagger} \boldsymbol{\omega}_k x_k + \sum_{\substack{n=1 \\ n\neq k}}^{K} \underbrace{\alpha_n \sqrt{P_s} h_{u,k} \boldsymbol{a}_{u,k}^{\dagger} \boldsymbol{\omega}_n x_n}_{\text{Leakage of User}n \text{ to User } k} + n_{u,k} \tag{12}$$

In Eq.(12), $h_{u,k}$ is the fading coefficient of the kth user. The signal is not contaminated by AN as $\boldsymbol{a}_{u,k}^{\dagger}\boldsymbol{P}_{\mathrm{AN}} = \boldsymbol{0}_{N-K}^{T}$, but it suffers from MAI. Therefore, the SINR of the kth user is

$$\mathrm{SINR}_{u,k} = \frac{\alpha_k^2 P_s \left|h_{u,k}\right|^2 \left|\boldsymbol{a}_{u,k}^{\dagger}\boldsymbol{\omega}_k\right|^2}{\sum\limits_{\substack{n=1 \\ n\neq k}}^{K} \alpha_n^2 P_s \left|h_{u,k}\right|^2 \left|\boldsymbol{a}_{u,k}^{\dagger}\boldsymbol{\omega}_n\right|^2 + \sigma_{u,k}^2} \tag{13}$$

Similarly, the received signal of the kth eavesdropper is

$$y_{e,k} = \sum_{n=1}^{K} \underbrace{\alpha_n \sqrt{P_s} h_{e,k} \boldsymbol{a}_{e,k}^{\dagger} \boldsymbol{\omega}_n x_n}_{\text{Leakage of User } n \text{ to Eve } k} + \underbrace{\alpha_{\mathrm{AN}} \sqrt{P_s} h_{e,k} \boldsymbol{a}_{e,k}^{\dagger} \boldsymbol{P}_{\mathrm{AN}} \boldsymbol{\mu}}_{\text{Artificial noise}} + n_{e,k} \tag{14}$$

Correspondingly, the signal-to-artificial-noise-ratio (SANR) of the kth eavesdroppers is given by

$$\mathrm{SANR}_{e,k} = \frac{N \sum_{n=1}^{K} \alpha_n^2 P_s \left|h_{e,k}\right|^2 \left|\boldsymbol{a}_{e,k}^{\dagger}\boldsymbol{\omega}_n\right|^2}{\alpha_{\mathrm{AN}}^2 P_s \left|h_{e,k}\right|^2 \boldsymbol{a}_{e,k}^{\dagger} \boldsymbol{P}_{\mathrm{AN}} \boldsymbol{P}_{\mathrm{AN}}^{\dagger} \boldsymbol{a}_{e,k} + N\sigma_{e,k}^2} \tag{15}$$

implicitly assuming that the eavesdropper can separately process the multi-stream signals. Note that this is a worst-case scenario for the proposed scheme. Hence in the multi-user downlink channel, the *sum secrecy rate* (SSR) of the FDA-DM system is

$$\mathrm{SR} = \sum_{k=1}^{K} \log_2\left(1+\mathrm{SINR}_{u,k}\right) - \max_{k} \log_2\left(1+\mathrm{SANR}_{e,k}\right) \tag{16}$$

To make full use of the transmission power, the beamforming vectors are based on the MRT, i.e., $\boldsymbol{\omega}_k = \frac{1}{\sqrt{N}}\boldsymbol{a}_{u,k}$, which are also widely used in other DM-based transmitters [7], [8], [26]. By doing so, we can focus on the optimization problem with respect only to the FOs of the FDA. We leave the problem of joint optimizing $\boldsymbol{\omega}_k$ and $\boldsymbol{f}$ as an open problem for the future studies. The expression of sum secrecy rate can be used as an optimization criterion for determining $\boldsymbol{f}$, i.e., to find the optimal FOs $\boldsymbol{f}^*$ that maximizes Eq.(16). However, this criterion still remains challenging as the target variables are coupled in the multiple components of the objective function. Moreover, all these components are non-convex w.r.t. $\boldsymbol{f}$. To avoid establishing an unsolvable problem, we introduce the measurement called *leakage* [27] to our FDA-DM system. The definition of leakage of the kth user is the power leaked from this user to all other users and the eavesdroppers known in advance, which can be mathematically expressed as

$$L_k = \alpha_k^2 P_s \sum_{\substack{n=1 \\ n\neq k}}^{K} \left|h_{u,n}\right|^2 \left|\boldsymbol{a}_{u,n}^{\dagger}\boldsymbol{\omega}_k\right|^2 + \alpha_k^2 P_s \sum_{n=1}^{E_n} \left|h_{e,n}\right|^2 \left|\boldsymbol{a}_{e,n}^{\dagger}\boldsymbol{\omega}_k\right|^2 \quad (17)$$

Using this concept, we can formulate an optimization problem which deals with the leakage power instead of dealing with the hard-to-solved secrecy rate maximization problem. Specifically, we would like to select the transmitting frequencies $\boldsymbol{f}$ to minimize the total leakage of all the users, so the optimization problem is given as

$$\begin{aligned} &\min_{f} \sum_{k=1}^{K} L_k \\ &\text{s.t. } 0 \le f_l - f_c \le \Delta F, \quad l \in \{1, \ldots, N\}. \end{aligned} \quad (18)$$

where ΔF is the maximum allowable FO. The physical meaning of the above problem is to reduce the signal energy of MAI and intercepted by the eavesdroppers as much as possible, so that the transmitter can increase the sum capacity of the legitimate users while reducing the eavesdroppers' achievable rate, and ultimately improve the security performance of the system.

B. ALGORITHM DESCRIPTION

We focus on solving the leakage minimization problem (18) in this subsection. The objective function of this problem is still non-convex, so it can not be solved by ordinary convex optimization methods. We deal with the objective function, which can be equivalently transformed as

$$\sum_{k=1}^{K} L_k \Leftrightarrow \sum_{k=1}^{K}\sum_{\substack{n=1 \\ n\neq k}}^{K} \alpha_k^2 \left|h_{u,n}\right|^2 \left|\boldsymbol{a}_{u,n}^{\dagger}\boldsymbol{a}_{u,k}\right|^2 + \sum_{k=1}^{K}\sum_{n=1}^{E_n} \alpha_k^2 \left|h_{e,n}\right|^2 \left|\boldsymbol{a}_{e,n}^{\dagger}\boldsymbol{a}_{u,k}\right|^2 \quad (19)$$

which consists of the inner products of the baseband steering vectors of the legitimate users and the known eavesdroppers. According to Eq.(6), the inner product of $\boldsymbol{a}(R_1, \theta_1, 0)$ and $\boldsymbol{a}(R_2, \theta_2, \tau)$ is given by

$$\boldsymbol{a}^{\dagger}(R_1, \theta_1, 0)\,\boldsymbol{a}(R_2, \theta_2, \tau) = \sum_{l=1}^{N} e^{j2\pi\left(f_c\frac{(l-1)d(\cos\theta_1-\cos\theta_2)}{c}+\Delta f_l\left(\frac{R_2-R_1}{c}-\tau\right)\right)} \quad (20)$$

Denoting $\varphi_l = \frac{(l-1)d(\cos\theta_1-\cos\theta_2)}{c} + \frac{R_2-R_1}{c} - \tau$, and utilizing $\Delta f_l \ll f_c$, the following equivalent transformations can be established

$$\begin{aligned} &\boldsymbol{a}^{\dagger}(R_1, \theta_1, 0)\,\boldsymbol{a}(R_2, \theta_2, \tau) \\ &\approx \sum_{l=1}^{N} e^{j2\pi\left(f_l\frac{(l-1)d(\cos\theta_1-\cos\theta_2)}{c}+\Delta f_l\left(\frac{R_2-R_1}{c}-\tau\right)\right)} \\ &\propto \sum_{l=1}^{N} e^{\mathrm{j}2\pi\left(f_l\frac{(l-1)d(\cos\theta_1-\cos\theta_2)}{c}+f_l\left(\frac{R_2-R_1}{c}-\tau\right)\right)} \\ &= \sum_{l=1}^{N} e^{\mathrm{j}2\pi f_l\varphi_l} \end{aligned} \quad (21)$$

Based on these transformations, we have

$$\begin{aligned} &\left|\boldsymbol{a}^{\dagger}(R_1, \theta_1, 0)\,\boldsymbol{a}(R_2, \theta_2, \tau)\right|^2 \\ &\Leftrightarrow \sum_{l_1=1}^{N}\sum_{l_2=1}^{N} e^{\mathrm{j}2\pi\left(f_{l_1}\varphi_{l_1}-f_{l_2}\varphi_{l_2}\right)} \\ &= N + 2\sum_{l_1=1}^{N}\sum_{l_2=l_1+1}^{N} \cos 2\pi\left(f_{l_1}\varphi_{l_1} - f_{l_2}\varphi_{l_2}\right) \\ &\Leftrightarrow \sum_{l_1=1}^{N}\sum_{\substack{l_2=1 \\ l_2\neq l_1}}^{N} \cos 2\pi\left(f_{l_1}\varphi_{l_1} - f_{l_2}\varphi_{l_2}\right) \end{aligned} \quad (22)$$

Consequently, the objective function of (18) can be equivalently transformed to

$$\begin{aligned} \sum_{k=1}^{K} L_k &\Leftrightarrow \sum_{k=1}^{K}\sum_{n\in\mathcal{S}_{UE}} \alpha_k^2 \left|h_n\right|^2 \left|\boldsymbol{a}_n^{\dagger}\boldsymbol{a}_{u,k}\right|^2 \Leftrightarrow g(\boldsymbol{f}) \\ &\triangleq \sum_{k=1}^{K}\sum_{n\in\mathcal{S}_{UE}} \left\{\alpha_k^2 \left|h_n\right|^2 \times \sum_{l_1=1}^{N}\sum_{l_2=l_1+1}^{N} \cos 2\pi\left(f_{l_1}\varphi_{kn,l_1} - f_{l_2}\varphi_{kn,l_2}\right)\right\} \end{aligned} \quad (23)$$

where $\mathcal{S}_{UE}$ represents the set of the subscripts for all legitimate users and known eavesdroppers, i.e., $\mathcal{S}_{UE} \triangleq \{(u,1), \ldots, (u,K), (e,1), \ldots, (e,E_n)\}$. Moreover, we define the notations $\varphi_{kn,l}$ as

$$\varphi_{kn,l} \triangleq \frac{(l-1)d\left(\cos\theta_{u,k} - \cos\theta_n\right)}{c} + \frac{R_n - R_{u,k}}{c} - \tau_n \quad (24)$$

With the transformed objective function in Eq.(23), the optimization program (18) can be iteratively solved by the

block successive upper-bound minimization (BSUM) algorithm [28]. This algorithm has also been used to solve similar optimization problems w.r.t. the FDA's FOs in [9], [13], [14]. However, all of them were based on the FDA's RF model, so the time-modulated beamforming weights had to be used. Moreover, there were errors in the upper bound functions and the stop conditions in these references. Therefore, this paper re-derives the BSUM algorithm for optimizing the FOs of the FDA.

According to the principle of BSUM, the algorithm begins from a feasible point $\boldsymbol{f}^0$. At each iteration, only one block is optimized, while other blocks are fixed. Based on that, we optimize f_m in the rth iteration by solving the following sub-problem

$$\begin{aligned} &\min_{f_m} g_r\left(f_m;\boldsymbol{f}_{-m}^{r-1}\right) \\ &\text{s.t. } 0 \le f_m - f_c \le \Delta F. \end{aligned} \tag{25}$$

where $\boldsymbol{f}_{-m}^{r-1} \in \mathbb{R}^{N-1}$ is the FO vector formed by removing the mth element from $\boldsymbol{f}$, and m is the remainder of $r \div N$. The objective function of the problem (25) is

$$\begin{aligned} &g_r\left(f_m;\boldsymbol{f}_{-m}^{r-1}\right) \\ &\quad\triangleq \sum_{k=1}^{K}\sum_{n\in\mathcal{S}_{UE}}\left\{\alpha_k^2\left|h_n\right|^2\sum_{\substack{l=1\\l\neq m}}^{N}\cos 2\pi\left(f_m\varphi_{kn,m}-f_l\varphi_{kn,l}\right)\right\} \end{aligned} \tag{26}$$

and it can be approximated by a quadratic function, denoted as

$$u_r\left(f_m;\boldsymbol{f}^{r-1}\right)=\sum_{k=1}^{K}\sum_{n\in\mathcal{S}_{UE}}\left\{\alpha_k^2\left|h_n\right|^2\sum_{\substack{l=1\\l\neq m}}^{N}\tilde{u}_{kn,l}\left(f_m;f_l^{r-1}\right)\right\} \tag{27}$$

where $\tilde{u}_{kn,l}\left(f_m;f_l^{r-1}\right)$ is the quadratic approximation function of $\tilde{g}_{kn,l}\left(f_m;f_l^{r-1}\right) \triangleq \cos 2\pi\left(f_m\varphi_{kn,m}-f_l^{r-1}\varphi_{kn,l}\right)$, and its expression is

$$\tilde{u}_{kn,l}\left(f_m;f_l^{r-1}\right)=\tilde{a}_{kn,l}\left(f_m-\tilde{c}_{kn,l}\right)^2+\tilde{b}_{kn,l} \tag{28}$$

Then, in the rth iteration, the problem (25) can be replaced by

$$\begin{aligned} &\min_{f_m} u_r\left(f_m;\boldsymbol{f}^{r-1}\right) \\ &\text{s.t. } 0 \le f_m - f_c \le \Delta F. \end{aligned} \tag{29}$$

which has an unique global optimal solution given as

$$f_m^r=\left\{\frac{\sum_{k=1}^{K}\sum_{n\in\mathcal{S}_{UE}}\sum_{\substack{l_2=1\\l_2\neq m}}^{N}\tilde{a}_{kn,l}\tilde{c}_{kn,l}}{\sum_{k=1}^{K}\sum_{n\in\mathcal{S}_{UE}}\sum_{\substack{l_2=1\\l_2\neq m}}^{N}\tilde{a}_{kn,l}}\right\}_{f_c}^{f_c+\Delta F} \tag{30}$$

At last, the final step of the rth iteration is to let $f_s^r = f_s^{r-1}, \forall s \neq m$. Repeat the above steps to optimize each variable in turn until the convergence condition is satisfied.

The prerequisite for the convergence of BSUM is that the quadratic approximation function in Eq.(27) needs to be carefully designed to satisfy certain conditions. According to the convergence description of BSUM, $u_r\left(f_m;\boldsymbol{f}^{r-1}\right)$ not only needs to be a quadratic function, but also to be a tight upper bound function of $g_r\left(f_m;\boldsymbol{f}_{-m}^{r-1}\right)$. This is equivalent to that for all k,n and l, $\tilde{u}_{kn,l}\left(f_m;f_l^{r-1}\right)$ constitutes a tight quadratic upper bound function of $\tilde{g}_{kn,l}\left(f_m;f_l^{r-1}\right)$ at $f_m = f_m^{r-1}$, which can be mathematically described as

$$\begin{cases} \tilde{u}_{kn,l}\left(f_m^{r-1};f_l^{r-1}\right)=\tilde{g}_{kn,l}\left(f_m^{r-1};f_l^{r-1}\right), \\ \tilde{u}_{kn,l}\left(f_m;f_l^{r-1}\right)\ge\tilde{g}_{kn,l}\left(f_m;f_l^{r-1}\right), \\ \tilde{u}'_{kn,l}\left(f_m^{r-1};f_l^{r-1}\right)=\tilde{g}'_{kn,l}\left(f_m^{r-1};f_l^{r-1}\right). \end{cases} \tag{31}$$

Besides, the geometric relationship between $\tilde{u}_{kn,l}\left(f_m;f_l^{r-1}\right)$ and $\tilde{g}_{kn,l}\left(f_m;f_l^{r-1}\right)$ is illustrated in Fig.19, which is given in Appendix A. It can be seen that the distance between $\tilde{c}_{kn,l}$ and f_m^{r-1} should be smaller than a quarter period of the original cosine function. Therefore, in order to get the correct coefficients, we also require that

$$\left|\tilde{c}_{kn,l}-f_m^{r-1}\right|<\frac{1}{2\left|\varphi_{kn,m}\right|} \tag{32}$$

By jointly solving the inequalities (31) and (32), the coefficients of the quadratic upper bound function $\tilde{u}_{kn,l}\left(f_m;f_l^{r-1}\right)$ can be obtained. That is, when $\tilde{g}'_{kn,l}\left(f_m^{r-1};f_l^{r-1}\right)=0$, we have

$$\begin{cases} \tilde{a}_{kn,l}=\left(1-\tilde{b}_{kn,l}\right)\pi^2\varphi_{kn,m}, \\ \tilde{b}_{kn,l}=\cos 2\pi\left(f_m^{r-1}\varphi_{kn,m}-f_l^{r-1}\varphi_{kn,l}\right), \\ \tilde{c}_{kn,l}=f_m^{r-1}. \end{cases} \tag{33}$$

When $\tilde{g}'_{kn,l}\left(f_m^{r-1};f_l^{r-1}\right)\neq 0$,

$$\begin{cases} \tilde{a}_{kn,l}=\dfrac{-\pi\varphi_{kn,m}\sin\ 2\pi\left(f_m^{r-1}\varphi_{kn,m}-f_l^{r-1}\varphi_{kn,l}\right)}{f_m^{r-1}-\tilde{c}_{kn,l}}, \\ \tilde{b}_{kn,l}=\cos 2\pi\left(f_m^{r-1}\varphi_{kn,m}-f_l^{r-1}\varphi_{kn,l}\right) \\ \qquad\qquad -\tilde{a}_{kn,l}\left(f_m^{r-1}-\tilde{c}_{kn,l}\right)^2, \\ \tilde{c}_{kn,l}=\begin{cases} \dfrac{\left|2f_m^{r-1}\varphi_{kn,m}-2f_l^{r-1}\varphi_{kn,l}\right|}{2\varphi_{kn,m}}+\dfrac{f_l^{r-1}\varphi_{kn,l}}{\varphi_{kn,m}}, \\ \quad\text{if } \operatorname{sgn}\left\{\varphi_{kn,m}\right\}\tilde{g}'_{kn,l}\left(f_m^{r-1};f_l^{r-1}\right)>0; \\ \dfrac{\left[2f_m^{r-1}\varphi_{kn,m}-2f_l^{r-1}\varphi_{kn,l}\right]}{2\varphi_{kn,m}}+\dfrac{f_l^{r-1}\varphi_{kn,l}}{\varphi_{kn,m}}, \\ \quad\text{if } \operatorname{sgn}\left\{\varphi_{kn,m}\right\}\tilde{g}'_{kn,l}\left(f_m^{r-1};f_l^{r-1}\right)<0. \end{cases} \end{cases} \tag{34}$$

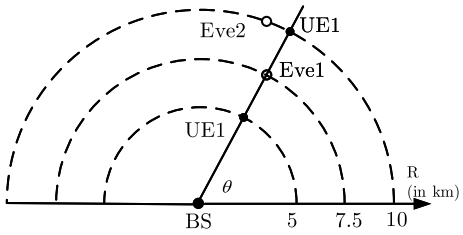

FIGURE 6. Simplified downlink multi-user wiretap channel.

The derivation of the above coefficients is given in Appendix A, while the strict proof that $\tilde{u}_{kn,l}\left(f_m; f_l^{r-1}\right)$ constitutes a tight upper bound function of $\tilde{g}_{kn,l}\left(f_m; f_l^{r-1}\right)$ is given in Appendix B. We would like to remind our readers to pay attention to the difference between Eq.(34) and Eq.(25) given in [9], which did not consider the case of $\varphi_{kn,m} < 0$. Similar mistakes also occurred in [13] and [14].

In Algorithm 1, the optimization algorithm w.r.t. the FDA's FOs is summarized. According to [28], the algorithm must converge to a stationary solution of (18). We should mention that as Eq.(30) is independent from $\tilde{b}_{kn,l}$, so the computational complexity can be reduced. Moreover, closed-form solutions can be obtained at each iteration, thus the algorithm can be efficiently performed.

Algorithm 1 Iterative BSUM Algorithm for Leakage Minimization Problem (18)

1: **Initialization**: Find a feasible point $\boldsymbol{f}^0$ and set $r = 0$. A small positive ϵ is chosen as the stopping criterion;
2: Calculate $\varphi_{kn,l}$ according to Eq.(24) and save them;
3: **Repeat**
4: $r = r + 1,\ m = (r \bmod N) + 1$;
5: Determine $\tilde{a}_{kn,l}$ and $\tilde{c}_{kn,l}$ by (33) and (34);
6: Calculate f_m^r according to (30);
7: $f_s^r = f_s^{r-1},\ \forall\, s \neq m$;
8: **Until** $r > N$ and $\|\boldsymbol{f}^r - \boldsymbol{f}^{r-N}\| \leq \epsilon$;
9: **Output**: the final optimal $\boldsymbol{f}^\star = \boldsymbol{f}^r$.

Remark 1: Although FDA-DM cannot provide absolute security in the range dimension, it still has some advantages over PA-DM. When FDA-DM is used, to obtain perfect eavesdropping, an eavesdropper needs to meet these requirements: 1) it is in the desired direction; 2) it needs to know all the sub-frequencies exactly; 3) it needs to be properly synchronized. In contrast, for PA-DM, eavesdroppers only need to meet the first condition to achieve perfect eavesdropping. Therefore, FDA-DM significantly increases the difficulty of eavesdropping in the legal direction, especially considering that AN is also superimposed on the useful signal.

V. NUMERICAL EXAMPLES

In this section, a simplified multi-user downlink model as illustrated in Fig.6 is adopted to demonstrate the security performance of the proposed MU-FDA-DM scheme, where

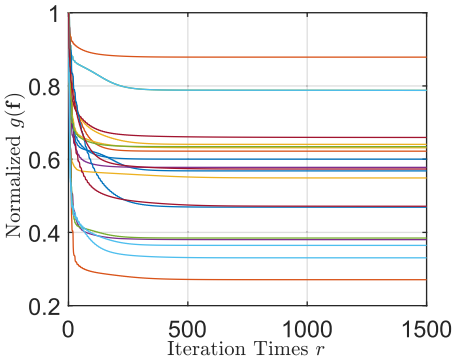

FIGURE 7. The converging behavior of BSUM.

the default parameters are set as follows. We consider line-of-sight (LOS) channels between the transmitter and all the receivers operating at $f_c = 10$GHz. There are two legitimate users (UE1,UE2) in the same direction, whose locations are (5km, 60°) and (10km, 60°) respectively. The locations of all the legitimate users are already known by the transmitter. Meanwhile, there exists at least one eavesdropper. The transmitter is equipped with an N-element array, where $N = 16$. The array spacing is always set as half of the minimum wavelength, i.e., $d = \frac{c}{2(f_c+\Delta F)}$, where the maximum allowable frequency offset ΔF is 1MHz. We define the efficiency of the transmission power as

$$\mathrm{PE} = \sum_{k=1}^{K} \alpha_k^2 \times 100\% \tag{35}$$

which represents the power ratio between the useful signal and the transmitted signal, and its default value is 80%. The total transmit power is set as 1 Watt, while α_k is the same for any k. The receive noise power is assumed to be -86dBm for all the users and eavesdroppers. The path fading coefficients h_n are determined by the free space path loss formula of radio wave propagation [9], i.e.,

$$h_n[\mathrm{dB}] = -32.5 - 20\lg f_c - 20\lg R_n \tag{36}$$

where the transmit frequency f_c is in megahertz (MHz), and the range R_n is in kilometer (km).

First of all, the converging behavior of Algorithm 1 is illustrated with 20 curves in Fig.7, where each curve starts from a randomly selected initial $\boldsymbol{f}^0$. In this simulation, there are two eavesdroppers located at (7.5km, 60°) and (10km, 62°) respectively, and their locations are known by the transmitter. The ZPTs of the two eavesdroppers are both 0, which means they are fully-synchronized. It can be seen that the value of $g(\boldsymbol{f}^r)$ decreases monotonically as r increases, and the BSUM algorithm converges in about 400 iterations.

In Fig.8, the 2-dimensional simulation results of the relationship between the achievable rate of a fully-synchronized receiver and its location in the MU-FDA-DM downlink channel are illustrated. Fig8-(a) and (b) respectively correspond to the situation where the eavesdroppers' CSI is unknown (i.e., $E_n = 0$) and known (i.e., $E_n = 2$), while other simulation conditions are the same as in Fig.7. In this two sub-figures,

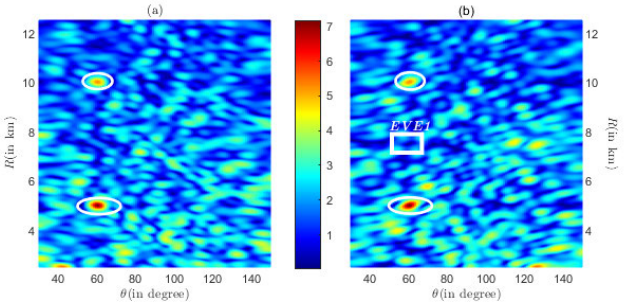

FIGURE 8. Achievable rate distribution versus the receiver's location.

the highest peaks of the surface correspond to the locations of two legitimate users. When the receiver is in other undesired positions, the achievable rate is reduced, which guarantees the effectiveness of the proposed scheme. Moreover, when the transmitter has a priori information of the eavesdroppers, the achievable rates at the eavesdroppers' locations can be further depressed via Algorithm 1.

To better demonstate the necessity of optimizing the FDA's FOs, we show how the FOs affects the security performance of the FDA-DM system through a series of experiments, which are illustrated from Fig.9 to Fig.16. In these experiments, the SSR curves of FDA-DM scheme equipped with other widely-used FOs are given as benchmarks, including *linear frequency offsets* (LFOs) [19], i.e., $\Delta f_l = (l-1)\Delta f$, *logarithmically increasing frequency offsets* (LogFOs) [18], i.e., $\Delta f_l = \Delta f \cdot \log_a l$ where a is 2 in our simulations, *random frequency offsets* (RFOs) [8], i.e., $\Delta f_l = \zeta_l \Delta F$ where ζ_l is a random variable obeying $U(0, 1)$, and PA, i.e., $\Delta f_l = 0$.

We first consider the case where there is only one unknown eavesdropper and illustrate how its location affects the SSR. In Fig.9, the relationship between SSR and R_e is given. In this experiment, the SSR provided by PA-DM is always 0, so it is not drawn. It can be seen that only when $\theta_e = 60°$, the SSR curve of our proposed scheme has two obvious **depressions** at the locations of the legal users. This first shows that perfect eavesdropping can only be achieved when the eavesdropper is in the desired direction. Second, it shows that if the eavesdroppers are fully synchronized, the FDA-DM scheme can achieve point-to-point secure communication.

On the other hand, when the eavesdropper is not fully synchronized with the transmitter, it is possible to eavesdrop on more information. From Fig.10 where $\theta_e = 60°$, we can see that the location of the depression changes according to τ_e, as the distance between the first two depressions is approximately 1km $\approx$ 3.3us $\times$ c. This shows that the eavesdroppers in the legal direction can perfectly eavesdrop on a legal user through proper synchronization, so the baseband model of the FDA does not violate physical laws. The SSR curve when the eavesdropper is properly synchronized with UE1 is also given in Fig.10. In this circumstance, the SSR is only provided by the UE2's achievable rate, thus it is lower than the other two cases.

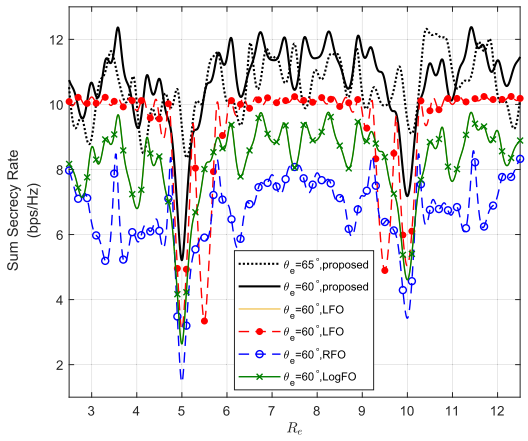

FIGURE 9. The SSR comparison for FDA-DM with different FOs versus R_e.

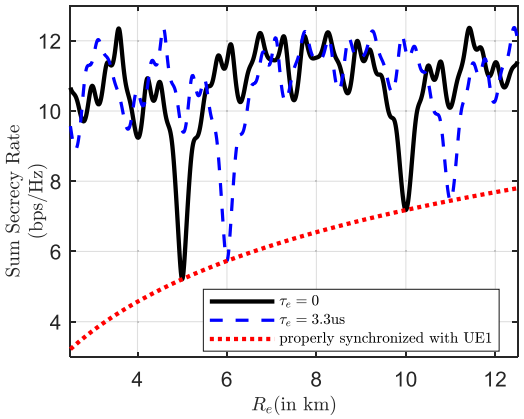

FIGURE 10. The SSR comparison for the proposed FDA-DM scheme versus R_e with different kinds of eavesdroppers, where $\theta_e = 60°$.

We can also see from Fig.9 that when the eavesdropper arrives at the location of a legitimate user, the proposed FDA-DM scheme can obtain the highest SSR. In this scenario, the SSR is equal to the achievable rate of another user, which means the MAI has been effectively suppressed through optimizing the FDA's FOs. Moreover, the proposed scheme provides the highest SSR except for a few places. In rare cases, the SSR of our scheme is slightly lower than LFO-FDA-DM. However, the SSR curve of LFO-FDA-DM generates multiple depressions at undesired distances, which means that LFO-FDA-DM suffers a severe information leak.

Remark 2: To briefly explain the limitation of LFOs, the achievable rate distribution of the LFO-FDA-DM scheme is given in Fig.11, where the simulation conditions are the same as Fig.8. The main lobe is S-shaped, which means that fully synchronized eavesdroppers at these locations can achieve perfect eavesdropping. This phenomenon is known as range-angle coupling/ambiguity [29], [30]. The much more serious problem is that since the peaks appear in all directions, an eavesdropper anywhere in the space can achieve perfect eavesdropping through proper synchronization. Therefore, LFO-FDA is not suitable for secure communications.

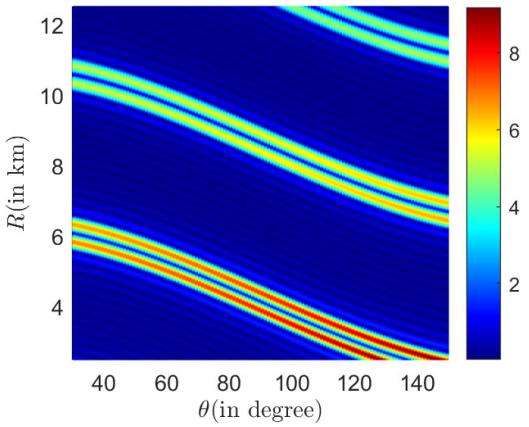

FIGURE 11. The achievable rate distribution of LFO-FDA-DM.

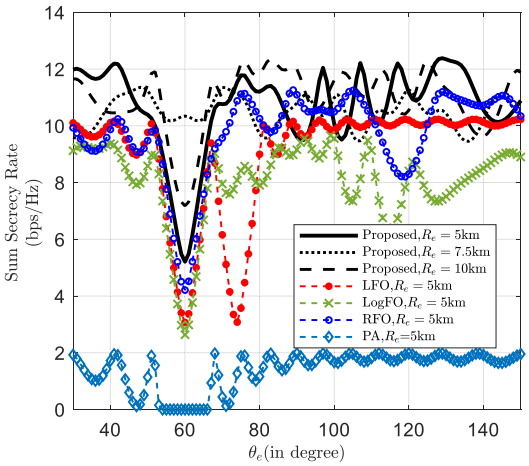

FIGURE 12. The SSR comparison for FDA-DM with different FOs versus θ_e.

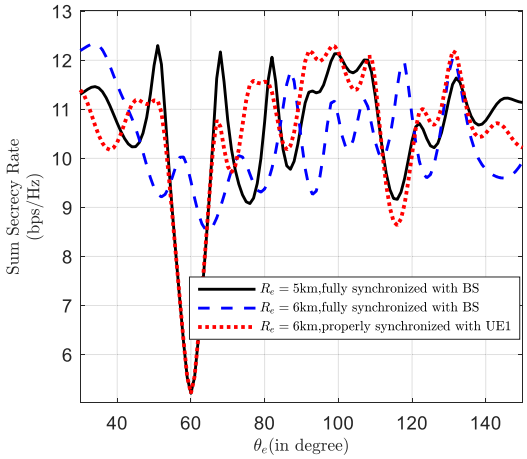

FIGURE 13. The SSR comparison for the proposed FDA-DM scheme versus θ_e with different kinds of eavesdroppers, where $R_e = 10$km.

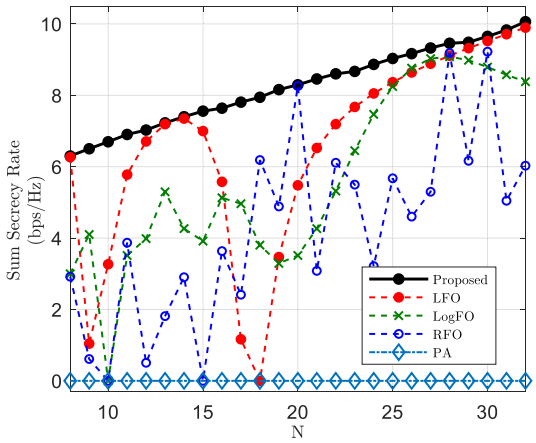

FIGURE 14. The SSR comparison for FDA-DM with different FOs versus N.

The relationship between SSR and θ_e is illustrated in Fig.12, where the eavesdropper is fully synchronized. Compared with PA-DM, FDA-DM can effectively increase the SSR in the multi-user network. Except for LFOs, the SSR curves of other FDA-DM transmitters are only recessed in the desired direction. In some directions, RFO-FDA-DM can provide higher SSR than the proposed scheme. But due to the randomness of RFOs, its performance is not stable. Moreover, the proposed scheme can still provide the highest SSR in most directions. Besides, Fig.13 shows that the security provided by FDA-DM in angle dimension is not affected by the ZPT of the eavesdropper, as even an eavesdropper which is properly synchronized with UE1 can achieve perfect eavesdropping only when $\theta_e = 60°$.

In the following two experiments, the influence of the FDA-DM transmitter's parameters on SSR is simulated, where two fully synchronized eavesdroppers are located at (7.5km, 60°) and (10km, 62°) while the transmitter does not know the existence of them. In Fig.14, the relationship between SSR and the number of transmitting antennas N is given. For an FDA-DM transmitter with fixed FOs, increasing the number of transmitting antennas may not necessarily lead to improved performance, and may even cause severe performance deterioration. However, the FDA-DM scheme based on FO optimization can make full use of the increased degrees of freedom provided by the array so monotonical increasing SSR is obtained. In Fig.15, the relationship between SSR and PE is given. We need to point out that when the simulation conditions change, the SSR curve of our proposed scheme will also change, instead of monotonically decreasing as PE decreases as shown in the figure. This is because for a lower PE, the eavesdropper will receive more AN, and its achievable rate is also reduced. So the SSR may still be improved, as shown by LFO-FDA-DM and LogFO-FDA-DM. However, unsurprisingly, PA-DM provides zero SSR in these two simulations, and FDA-DM with optimized FOs provides higher SSR than that with other FOs. These two experiments fully verify the effectiveness and necessity of optimizing the FDA's FOs.

When the number of eavesdroppers increases, the FDA-DM with optimized FOs also outperforms other benchmarks. The SSR of the FDA-DM versus E is given in Fig.16. We select 32 randomly-located fully-synchronized

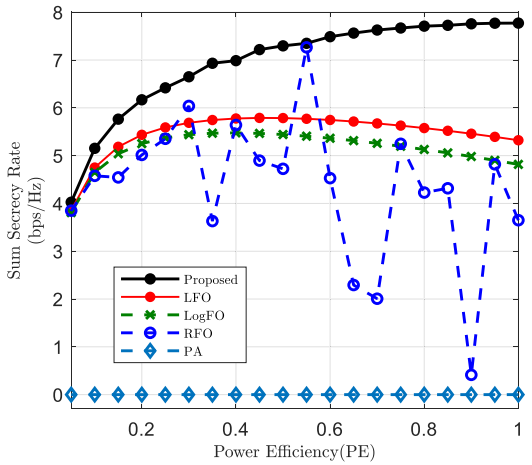

FIGURE 15. The SSR comparison for FDA-DM with different FOs versus PE.

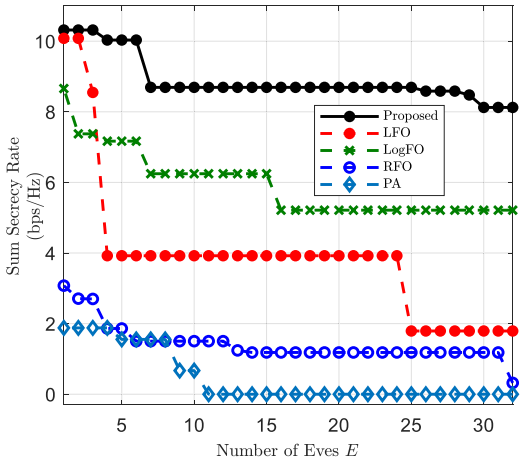

FIGURE 16. The SSR comparison for FDA-DM with different FOs versus the number of eavesdroppers E.

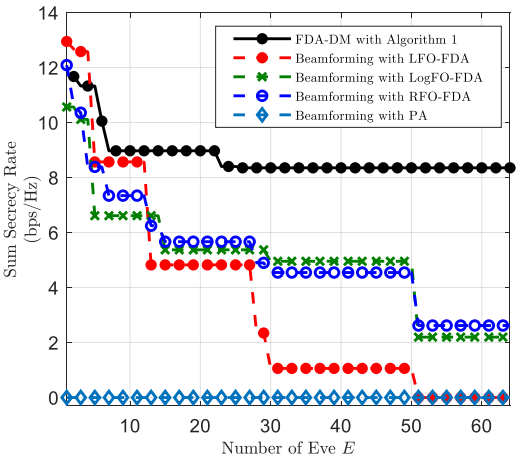

FIGURE 17. The SSR comparison between FDA-DM and beamforming versus the number of eavesdroppers E.

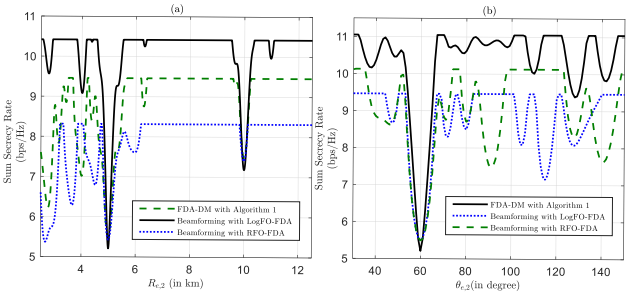

FIGURE 18. The SSR comparison between FDA-DM and beamforming versus the second eavesdropper's location, where $\theta_{e,2} = 60°$ in (a), and $R_{e,2} = 5$km in (b).

eavesdroppers, whose locations are not known by the transmitter. With the increase of E, the SSR curves of PA-DM and FDA-DM based on fixed FOs decrease rapidly, while the SSR of the proposed scheme decreases significantly slower. In addition, as with the other simulation results, the proposed scheme achieves the best security performance among all these schemes. This shows that optimizing FOs through Algorithm 1 makes FDA-DM more resistant to unknown eavesdroppers.

To compare the proposed FDA-DM scheme with beamforming, the beamforming scheme based on the *signal-to-leakage-noise-ratio* (SLNR) maximization criterion proposed in [24] is selected as the benchmark, which is proved to be effective in MU-MIMO downlink channels and has been widely used in many studies [31], [32]. When the eavesdropper's CSI is known, the beamforming method can also effectively reduce the eavesdropper's achievable rate [33]. However, when the CSI of the eavesdroppers is not known, FDA-DM can obtain better secure performance than beamforming. In Fig.17, the SSR comparison between the proposed FDA-DM and beamforming based on SLNR maximization versus E is given, where we select 64 unexposed randomly-located fully-synchronized eavesdroppers. Although the beamforming method obtains a slightly higher SSR when E is small, the security performance provided by the proposed FDA-DM scheme surpasses the beamforming method very quickly with the growth of E.

To better demonstrate the advantage of the proposed FDA-DM scheme over beamforming, another two numerical examples are given in Fig.18. In these two simulations, there are two unexposed fully-synchronized eavesdroppers. The location of the first eavesdropper is fixed at $(7.5\text{km}, 60°)$, while the relationship between SSR and the second eavesdropper's location is studied. Obviously, the proposed FDA-DM scheme provides higher SSR than the beamforming schemes in most cases. Fig.17 and Fig.18 illustrate that the proposed FDA-DM scheme outperforms the beamforming scheme based on maximizing SLNR. It should be noted that the SSR curves of the beamforming method based on PA and LFO-FDA are not given in Fig.18 due to their limitations in secure communications.

VI. CONCLUSION

In this paper, a novel FDA-DM scheme for multi-user downlink wiretap channels was proposed, where independent data streams were sent to different users. We developed this

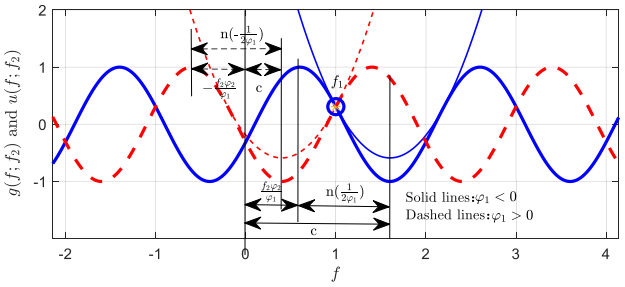

FIGURE 19. The geometric relationship between $u(f;f_2)$ and $g(f;f_2)$.

scheme based on the baseband model of the FDA, which solved the troubles brought by the time-varying nature of the FDA and provided a new direction for future researches. Based on the new model, the concept of LDMA was proposed preliminarily. LDMA can provide much higher system capacity when multiple users are in the same or proximal locations, without the need of time division, frequency division, or code division. In the FDA-DM scheme, based on the leakage minimization criterion, the carrier frequencies of the FDA were optimized through the BSUM algorithm, which gave a closed-form solution in each iteration thus could be effectively performed. Numerical results demonstrated that our proposed scheme could provide higher SSR than other DM schemes. Moreover, it showed better resistance to unknown eavesdroppers than the beamforming method based on the SLNR maximization criterion.

APPENDIX A

In Appendix A and B, we will derive the coefficients of the quadratic upper bound of the cosine function based on the inequalities (31) and (32). First of all, we drop the superscripts and the subscripts for notation simplicity and rewrite (31) and (32) as

$$\begin{cases} u\left(f_1;f_2\right)=g\left(f_1;f_2\right), \\ u\left(f;f_2\right)\geq g\left(f;f_2\right), \\ u'\left(f_1;f_2\right)=g'\left(f_1;f_2\right), \\ |c-f_1|\leq \dfrac{1}{2\left|\varphi_1\right|}. \end{cases} \tag{37}$$

where f corresponds to f_m, f_1 to f_m^{r-1}, f_2 to f_l^{r-1}, φ_1 to $\varphi_{kn,m}$, φ_2 to $\varphi_{kn,l}$, and[1]

$$g\left(f,f_2\right)=\cos 2\pi\left(f\varphi_1-f_2\varphi_2\right) \tag{38}$$

$$u\left(f,f_2\right)=a(f-c)^2+b \tag{39}$$

Based on the first and the third equalities of (37), we can get

$$-2\pi\varphi_1\sin 2\pi\left(f_1\varphi_1-f_2\varphi_2\right)=2a\left(f_1-c\right) \tag{40}$$

$$b=\cos 2\pi\left(f_1\varphi_1-f_2\varphi_2\right)-a\left(f_1-c\right)^2 \tag{41}$$

The following discussion needs to be divided into two cases. The first case is when $f_1-c\neq 0$, Eq.(40) can be revised as

$$a=\frac{-\pi\varphi_1\sin 2\pi\left(f_1\varphi_1-f_2\varphi_2\right)}{f_1-c} \tag{42}$$

Therefore, we only need to determine c in this case. To get the expression of c, the geometric relationship between $u(f;f_2)$ and $g(f;f_2)$ is illustrated in Fig.19. In this figure, n is an integer, which should satisfy the following inequalities

$$\begin{cases} 0\leq f_1-\dfrac{f_2\varphi_2}{\varphi_1}-\dfrac{n}{2\left|\varphi_1\right|}\leq\dfrac{1}{2\left|\varphi_1\right|}, & \text{if } g'(f_1;f_2)>0; \\ 0\leq\dfrac{n}{2\left|\varphi_1\right|}+\dfrac{f_2\varphi_2}{\varphi_1}-f_1\leq\dfrac{1}{2\left|\varphi_1\right|}, & \text{if } g'(f_1;f_2)<0. \end{cases} \tag{43}$$

Therefore, the expression of n can be derived as

$$n=\begin{cases} \lfloor 2f_1\left|\varphi_1\right|-2\,\mathrm{sgn}\left\{\varphi_1\right\}f_2\varphi_2\rfloor, & \text{if } g'(f_1;f_2)>0; \\ \lceil 2f_1\left|\varphi_1\right|-2\,\mathrm{sgn}\left\{\varphi_1\right\}f_2\varphi_2\rceil, & \text{if } g'(f_1;f_2)<0. \end{cases} \tag{44}$$

Utilizing $\lceil -a\rceil=-\lfloor a\rfloor$, (44) is equivalent to

$$n=\begin{cases} \mathrm{sgn}\left\{\varphi_1\right\}\lfloor 2f_1\varphi_1-2f_2\varphi_2\rfloor, \\ \qquad \text{if } \mathrm{sgn}\left\{\varphi_1\right\}\cdot g'\left(f_1;f_2\right)>0; \\ \mathrm{sgn}\left\{\varphi_1\right\}\lceil 2f_1\varphi_1-2f_2\varphi_2\rceil, \\ \qquad \text{if } \mathrm{sgn}\left\{\varphi_1\right\}\cdot g'\left(f_1;f_2\right)<0. \end{cases} \tag{45}$$

Consequently, utilizing $|a|=\mathrm{sgn}\{a\}\cdot a$, the expression of c in this case is given as

$$\begin{aligned} c&=\frac{n}{2\left|\varphi_1\right|}+\frac{f_2\varphi_2}{\varphi_1} \\ &=\begin{cases} \dfrac{\lfloor 2f_1\varphi_1-2f_2\varphi_2\rfloor}{2\varphi_1}+\dfrac{f_2\varphi_2}{\varphi_1}, \\ \qquad \text{if } \mathrm{sgn}\left\{\varphi_1\right\}\cdot g'\left(f_1;f_2\right)>0; \\ \dfrac{\lceil 2f_1\varphi_1-2f_2\varphi_2\rceil}{2\varphi_1}+\dfrac{f_2\varphi_2}{\varphi_1}, \\ \qquad \text{if } \mathrm{sgn}\left\{\varphi_1\right\}\cdot g'\left(f_1;f_2\right)<0. \end{cases} \end{aligned} \tag{46}$$

In another case when $f_1-c=0$, it is easy to verify that $g'(f_1;f_2)=0$ and $b=\cos 2\pi\left(f_1\varphi_1-f_2\varphi_2\right)\in\{-1,1\}$. If $b=1$, $u(f;f_2)=1$ is a solution for the inequalities (37). Otherwise, in order for $u(f;f_2)$ to form the upper bound of $g(f;f_2)$, the second derivative of $u(f;f_2)$ should be no less than that of $g(f;f_2)$ at $f=f_1$, i.e., $u(f;f_2)\geq g(f;f_2)$. Therefore, the following inequality holds

$$2a\geq -4\pi^2\varphi_1^2\cos 2\pi\left(f_1\varphi_1-f_2\varphi_2\right)=4\pi^2\varphi_1^2 \tag{47}$$

By taking the equal sign of the above inequality, a feasible solution of a is derived. Therefore, in the second case, we have $a=(1-b)\pi^2\varphi_1^2$.

In summary, the coefficients of $u(f;f_2)$ are:

1) When $g'(f_1;f_2)=0$,

$$\begin{cases} a=(1-b)\pi^2\varphi_1^2 \\ b=\cos 2\pi\left(f_1\varphi_1-f_2\varphi_2\right) \\ c=f_1 \end{cases} \tag{48}$$

[1]These symbols are dedicated in the appendices, as they have different meanings in the main text.

2) When $g'(f_1;f_2)\neq 0$,

$$\begin{cases} a=\dfrac{-\pi\varphi_1 \sin\ 2\pi\ (f_1\varphi_1-f_2\varphi_2)}{f_1-c} \\ b=\cos 2\pi\ (f_1\varphi_1-f_2\varphi_2)-a\,(f_1-c)^2 \\ c=\begin{cases} \dfrac{\lfloor 2f_1\varphi_1-2f_2\varphi_2\rfloor}{2\varphi_1}+\dfrac{f_2\varphi_2}{\varphi_1}, \\ \quad \text{if } \operatorname{sgn}\{\varphi_1\}\cdot g'\,(f_1;f_2)>0; \\ \dfrac{\lceil 2f_1\varphi_1-2f_2\varphi_2\rceil}{2\varphi_1}+\dfrac{f_2\varphi_2}{\varphi_1}, \\ \quad \text{if } \operatorname{sgn}\{\varphi_1\}\cdot g'\,(f_1;f_2)<0. \end{cases} \end{cases} \tag{49}$$

APPENDIX B

In this appendix, we will strictly prove that $u(f;f_2)$ derived from the geometric relationship forms a upper bound of $g(f;f_2)$. The proof is divided into the following cases:

1) When $u(f_1;f_2)=1$, it is obvious that $u(f;f_2)=1\geq g(f;f_2)$;

2) When $u(f_1;f_2)=-1$, $g''(f_1;f_2)\geq g''(f;f_2)$, $\forall f$. Moreover, as $g''(f_1;f_2)=u''(f_1;f_2), u''(f;f_2)\geq g''(f;f_2)$, $\forall f>f_1$. Then, $u'(f;f_2)\geq g'(f;f_2)$, $\forall f>f_1$ because $u'(f_1;f_2)=g'(f_1;f_2)$. Therefore, $u(f;f_2)\geq g(f;f_2)$, $\forall f>f_1$ because $u(f_1;f_2)=g(f_1;f_2)$. Similarly, we can prove that $u(f;f_2)\geq g(f;f_2)$, $\forall f<f_1$.

3) For other cases, without loss of generality, we consider the situation when $\varphi_1>0$ and $g'(f_1;f_2)>0$. First, it can be seen from Fig.19 that we only need to prove that $u(f;f_2)\geq g(f;f_2)$ in the interval $\left(c-\frac{1}{2|\varphi_1|},c+\frac{1}{2|\varphi_1|}\right)$. This proposition can proved by the following steps:

Condition 1: $u'\,(f;f_2)=2\frac{-\pi\varphi_1\sin\ 2\pi(f_1\varphi_1-f_2\varphi_2)}{f_1-c}(f-c)$ is a linear funtion of f, and $u'(c;f_2)=g'(c;f_2)=0$, $u'(f_1;f_2)=g'(f_1;f_2)$.

Condition 2: In the interval $\left(c,c+\frac{1}{2\varphi_1}\right)$, $g'\,(f;f_2)=-\pi\varphi_1\sin\ 2\pi\,(f\varphi_1-f_2\varphi_2)>0$ is concave.

$\Rightarrow$ Therefore, $\forall f_1\in\left(c,c+\frac{1}{2\varphi_1}\right)$, $u'(f;f_2)<g'(f;f_2)$ when $f\in(c,f_1)$, and $u'(f;f_2)>g'(f;f_2)$ when $f\in\left(f_1,c+\frac{1}{2\varphi_1}\right)$.

Condition 3: $u(f_1;f_2)=g(f_1;f_2)$.

Condition 4: Both $u(f;f_2)$ and $g(f;f_2)$ are monotonically increasing in the interval $\left(c,c+\frac{1}{2\varphi_1}\right)$.

$\Rightarrow$ Therefore, $u(f;f_2)\geq g(f;f_2)$ when $f\in\left(c,c+\frac{1}{2\varphi_1}\right)$. The equality holds only when $f=f_1$.

Condition 5: $u(f;f_2)$ and $g(f;f_2)$ are evenly symmetric about $f=c$.

$\Rightarrow u(f;f_2)\geq g(f;f_2)$ also holds when $f\in\left(c-\frac{1}{2\varphi_1},c\right)$.

$\Rightarrow$ When $f\in\left(c-\frac{1}{2\varphi_1},c+\frac{1}{2\varphi_1}\right)$, $u(f;f_2)\geq g(f;f_2)$.

Similar proof can be applied to the situations when $\varphi_1<0$ or $g'(f_1;f_2)<0$. Therefore, we have completed the proof.

REFERENCES

[1] A. Kolling, P. Walker, N. Chakraborty, K. Sycara, and M. Lewis, "Human interaction with robot swarms: A survey," *IEEE Trans. Human-Machine Syst.*, vol. 46, no. 1, pp. 9–26, Feb. 2016.
[2] Y. Zhang, G. Tian, J. Lu, M. Zhang, and S. Zhang, "Efficient dynamic object search in home environment by mobile robot: *A priori* knowledge-based approach," *IEEE Trans. Veh. Technol.*, vol. 68, no. 10, pp. 9466–9477, Oct. 2019.
[3] C. Chen, S. Wang, L. Li, S. Ke, C. Wang, and X. Bu, "Intelligent covert satellite communication for military robot swarm," *IEEE Access*, vol. 8, pp. 5363–5382, 2020.
[4] S. Luo, S. Zhang, S. Ke, S. Wang, X. Bu, and J. An, "Optimum combining for coherent FFH/DS spread spectrum receivers in the presence of multi-tone jammer," *IEEE Access*, vol. 8, pp. 53097–53106, 2020.
[5] Y. Wu, B. Zhang, X. Yi, and Y. Tang, "Collaborative communication in multi-robot surveillance based on indoor radio mapping," in *Proc. Int. Conf. Collaborative Comput., Netw., Appl. Worksharing*. Cham, Switzerland: Springer, 2016, pp. 211–220.
[6] J. Zhang, T. Chen, S. Zhong, J. Wang, W. Zhang, X. Zuo, R. G. Maunder, and L. Hanzo, "Aeronautical Ad Hoc networking for the Internet-above-the-clouds," *Proc. IEEE*, vol. 107, no. 5, pp. 868–911, May 2019.
[7] W.-Q. Wang, "DM using FDA antenna for secure transmission," *IET Microw., Antennas Propag.*, vol. 11, no. 3, pp. 336–345, Feb. 2017.
[8] J. Hu, S. Yan, F. Shu, J. Wang, J. Li, and Y. Zhang, "Artificial-noise-aided secure transmission with directional modulation based on random frequency diverse arrays," *IEEE Access*, vol. 5, pp. 1658–1667, 2017.
[9] J. Lin, Q. Li, J. Yang, H. Shao, and W.-Q. Wang, "Physical-layer security for proximal legitimate user and eavesdropper: A frequency diverse array beamforming approach," *IEEE Trans. Inf. Forensics Security*, vol. 13, no. 3, pp. 671–684, Mar. 2018.
[10] Y. Ding, A. Narbudowicz, and G. Goussetis, "Physical limitation of range-domain secrecy using frequency diverse arrays," *IEEE Access*, vol. 8, pp. 63302–63309, 2020.
[11] A.-M. Yao, W. Wu, and D.-G. Fang, "Frequency diverse array antenna using time-modulated optimized frequency offset to obtain time-invariant spatial fine focusing beampattern," *IEEE Trans. Antennas Propag.*, vol. 64, no. 10, pp. 4434–4446, Oct. 2016.
[12] K. Chen, S. Yang, Y. Chen, and S.-W. Qu, "Accurate models of time-invariant beampatterns for frequency diverse arrays," *IEEE Trans. Antennas Propag.*, vol. 67, no. 5, pp. 3022–3029, May 2019.
[13] B. Qiu, J. Xie, L. Wang, and Y. Wang, "Artificial-noise-aided secure transmission for proximal legitimate user and eavesdropper based on frequency diverse arrays," *IEEE Access*, vol. 6, pp. 52531–52543, 2018.
[14] B. Qiu, M. Tao, L. Wang, J. Xie, and Y. Wang, "Multi-beam directional modulation synthesis scheme based on frequency diverse array," *IEEE Trans. Inf. Forensics Security*, vol. 14, no. 10, pp. 2593–2606, Oct. 2019.
[15] T. C. Yang and W.-B. Yang, "Low probability of detection underwater acoustic communications using direct-sequence spread spectrum," *J. Acoust. Soc. Amer.*, vol. 124, no. 6, pp. 3632–3647, Dec. 2008.
[16] A.-M. Yao, P. Rocca, W. Wu, A. Massa, and D.-G. Fang, "Synthesis of time-modulated frequency diverse arrays for short-range multi-focusing," *IEEE J. Sel. Topics Signal Process.*, vol. 11, no. 2, pp. 282–294, Mar. 2017.
[17] X. Wei, Y. Xiao, Y. Xiao, Q. You, and W. Chen, "Spatial and directional modulation with random frequency diverse array," in *Proc. IEEE 8th Annu. Comput. Commun. Workshop Conf. (CCWC)*, Jan. 2018, pp. 976–979.
[18] Q. Cheng, J. Zhu, T. Xie, J. Luo, and Z. Xu, "Time-invariant angle-range dependent directional modulation based on time-modulated frequency diverse arrays," *IEEE Access*, vol. 5, pp. 26279–26290, 2017.
[19] J. Xu, G. Liao, S. Zhu, L. Huang, and H. C. So, "Joint range and angle estimation using MIMO radar with frequency diverse array," *IEEE Trans. Signal Process.*, vol. 63, no. 13, pp. 3396–3410, Jul. 2015.
[20] S. Ji, W.-Q. Wang, H. Chen, and S. Zhang, "On physical-layer security of FDA communications over Rayleigh fading channels," *IEEE Trans. Cognit. Commun. Netw.*, vol. 5, no. 3, pp. 476–490, Sep. 2019.
[21] S. Ji and W.-Q. Wang, "Physical-layer security for frequency diverse array communication system over Nakagami-m fading channels," *IEEE Syst. J.*, early access, Jul. 1, 2019, doi: 10.1109/JSYST.2019.2923103.
[22] J. Zhang, S. Chen, X. Mu, and L. Hanzo, "Turbo multi-user detection for OFDM/SDMA systems relying on differential evolution aided iterative channel estimation," *IEEE Trans. Commun.*, vol. 60, no. 6, pp. 1621–1633, Jun. 2012.
[23] J. Zhang, S. Chen, X. Mu, and L. Hanzo, "Evolutionary-algorithm-assisted joint channel estimation and turbo multiuser detection/decoding for OFDM/SDMA," *IEEE Trans. Veh. Technol.*, vol. 63, no. 3, pp. 1204–1222, Mar. 2014.
[24] M. Sadek, A. Tarighat, and A. Sayed, "A leakage-based precoding scheme for downlink multi-user MIMO channels," *IEEE Trans. Wireless Commun.*, vol. 6, no. 5, pp. 1711–1721, May 2007.

[25] Y. Xu, W. Li, and W. Qin, "The test and evaluation of GPS onboard clock," in *Proc. Joint Eur. Freq. Time Forum Int. Freq. Control Symp. (EFTF/IFC)*, Jul. 2013, pp. 295–298.
[26] Y. Ding and V. F. Fusco, "A vector approach for the analysis and synthesis of directional modulation transmitters," *IEEE Trans. Antennas Propag.*, vol. 62, no. 1, pp. 361–370, Jan. 2014.
[27] A. Tarighat, M. Sadek, and A. H. Sayed, "A multi user beamforming scheme for downlink MIMO channels based on maximizing signal-to-leakage ratios," in *Proc. IEEE Int. Conf. Acoust., Speech, Signal Process. (ICASSP)*, vol. 3, Mar. 2005, pp. iii/1129–iii/1132.
[28] M. Razaviyayn, M. Hong, and Z.-Q. Luo, "A unified convergence analysis of block successive minimization methods for nonsmooth optimization," *SIAM J. Optim.*, vol. 23, no. 2, pp. 1126–1153, Jan. 2013.
[29] J. Xiong, W.-Q. Wang, H. Shao, and H. Chen, "Frequency diverse array transmit beampattern optimization with genetic algorithm," *IEEE Antennas Wireless Propag. Lett.*, vol. 16, pp. 469–472, 2017.
[30] K. Gao, W.-Q. Wang, H. Chen, and J. Cai, "Transmit beamspace design for multi-carrier frequency diverse array sensor," *IEEE Sensors J.*, vol. 16, no. 14, pp. 5709–5714, Jul. 2016.
[31] V. R. Cadambe and S. A. Jafar, "Interference alignment and degrees of freedom of the K-user interference channel," *IEEE Trans. Inf. Theory*, vol. 54, no. 8, pp. 3425–3441, Aug. 2008.
[32] C. Shen, "Downlink multi-user MIMO precoding design via signal-over-leakage capacity," *IEEE Access*, vol. 6, pp. 2812–2824, 2018.
[33] M. S. Mohammadi, "MIMO minimum leakage—Physically secure wireless data transmission," in *Proc. Int. Conf. Appl. Inf. Commun. Technol.*, Oct. 2009, pp. 1–5.

SHENG KE (Graduate Student Member, IEEE) received the bachelor's degree in information engineering from the Beijing Institute of Technology (BIT), Beijing, China, in 2013. He is currently pursuing the Ph.D. degree with the School of Information and Electronics Communication, BIT. He was a Research Assistant with the University of Macau, from May 2018 to May 2020. His research interests include wireless communication, physical-layer security, and optimization theory. He was a Reviewer for the IEEE TRANSACTIONS ON VEHICULAR TECHNOLOGY, the IEEE TRANSACTIONS ON WIRELESS COMMUNICATIONS, and the IEEE International Conference on Communication Systems.

MINJUE HE received the master's degree in electronic engineering from the University of Electronic Science and Technology of China, in 2006. She is currently with the Science and Technology on Electronic Information Control Laboratory. Her research interests include low or zero power operations, swarm operations, swarm tactical networks, and multitime-space-frequency precise synchronization technology. She was awarded as an Expert of Office of Information Systems, Equipment Development Department, China.

XIANGYUAN BU (Member, IEEE) received the B.Eng. and Ph.D. degrees from the Beijing Institute of Technology (BIT), Beijing, China, in 1987 and 2007, respectively. From 1996 to 1998, he was a Visiting Scholar with the Military Academy of Belarus, Belarus. Since 2002, he has been with the School of Information and Electronics, BIT, where he is currently a Professor. His current research interests include wireless communication, digital signal processing, and channel coding.

WENLONG CAI received the Ph.D. degree from the School of Electronic and Information Engineering, Beihang University, China, in 2016. He is currently with the National Key Laboratory of Science and Technology on Aerospace Intelligence Control, Beijing Aerospace Automatic Control Institute. His research interests include information theory and signal processing methods for wireless communications, such as massive-MIMO communications, millimeter wave communications, and physical-layer security.